Journal of Water Process Engineering 36 (2020) 101306

Contents lists available at ScienceDirect

Journal of Water Process Engineering

journal homepage: www.elsevier.com/locate/jwpe

Assessment of the optimized treatment of indigo-polluted industrial textile wastewater by a sequential electrocoagulation-activated carbon adsorption process

Edison GilPavas*, Santiago Correa-Sanchez

GIPAB: Grupo de Investigación en Procesos Ambientales, Departamento de Ingeniería de Procesos, Universidad EAFIT, Cr 49 # 7 Sur 50, Medellín, Colombia

ARTICLE INFO

Keywords:
Textile wastewater
indigo
optimization
electrocoagulation
activated carbon
toxicity

ABSTRACT

Wastewater collected from a local jean manufacturing plant was treated using an electrocoagulation process (EC) coupled with activated carbon (AC) adsorption. The process variables were optimized using multivariate regression coupled with nonlinear programming with nonlinear restrictions to achieve the lowest possible cost while keeping a high enough degradation rate for chemical oxygen demand (COD), color, and turbidity to fulfill the Colombian environmental regulation requirements. Under optimal conditions (pH = 5.4, σ = 2 mS/cm, j = 14 mA/cm^2, and t = 11 min) color, COD, and TOC removals of 95%, 63%, and 51%, respectively, were achieved. The biodegradability index also increased from 0.13 to 0.29, whereas toxicity tests showed a remaining toxicity of 45%. A kinetic study was conducted for the EC process. The activated carbon (AC) adsorption process was successfully used to completely remove toxicity, while further increasing color, COD, and TOC removals to 96%, 72%, and 61%, respectively. The conditions for the AC adsorption process (20 g/L of AC and 1 h) were determined by experimental adsorption isotherms and kinetic studies. The optimized EC/AC process led to an effluent satisfying the Colombian regulations and seems technologically viable with lower costs than other similar process that were reported in previous works.

1. Introduction

In recent years, the textile industry has been a focus of environmental concern because of the large amounts of water it uses and the high quantities of wastewater it produces [1–3]. Textile industrial wastewater (TIWW) generated by textile manufacturing contains various dyes and a diverse array of other chemicals (e.g., fabric softeners, salts, pesticides, coupling agents, polishing and coating agents, and surfactants), composing a complex matrix with low biodegradability that may cause severe environmental impacts because of the toxicity of its components [4,5]. Conventional treatment is not viable for TIWW because of its complexity, thus only treatments based on more complex reactions can effectively remove pollutants in such matrices [1,6].

As reported in previous research [7,8], chemical coagulation can remove approximately half of the pollutants in TIWW. However, the outcome of chemical coagulation is very sensitive to changes in TIWW's organic load, which is highly variable over time. Therefore, this kind of approach is prone to coagulant overdoses or underdoses that lead to inefficiencies of the process. Additionally, coagulants often consist of iron and aluminum salts, thus adding coagulants can become a secondary source of pollution.

The electrocoagulation (EC) process has been studied as a response to these inconveniences [9–17]. In the EC process, the oxidation of a sacrificial anode in the presence of an external electrical current leads to the dissolution of Fe^{2+} (Eq. (1)), which reacts with OH- formed on the cathode (Eq. (2)), thus forming iron hydroxides that act as coagulant agents. Between pH values of 5.5 and 9.5, $Fe(OH)_2$ precipitates (Eq. (3)), and $Fe(OH)_3$ is formed by the oxidation of Fe^{2+} in the presence of dissolved $O_2(_g)$ (Eq.(4)), with released protons then reduced to H_2 gas (Eq. (5)). The summarized reaction for this process is presented in Eq. (6) [1].

$$Fe \rightarrow Fe^{2+} + 2e^- \tag{1}$$

$$2H_2O + 2e^- \rightarrow 2OH^- + H_{2(g)} \tag{2}$$

$$Fe^{2+} + 2OH^- \rightarrow Fe(OH)_{2(s)} \tag{3}$$

$$4Fe^{2+} + 10H_2O + O_{2(g)} \rightarrow 4Fe(OH)_{3(s)} + 8H^+ \tag{4}$$

$$8H^+ + 8e^- \rightarrow 4H_{2(g)} \tag{5}$$

* Corresponding author.
E-mail address: egil@eafit.edu.co (E. GilPavas).

https://doi.org/10.1016/j.jwpe.2020.101306
Received 13 January 2020; Received in revised form 15 April 2020; Accepted 17 April 2020
Available online 05 May 2020
2214-7144/

$$4Fe + 10H_2O + O_{2(g)} \rightarrow 4Fe(OH)_{3(s)} + 5H_{2(g)} \tag{6}$$

This approach can be conducted without the direct addition of chemical agents, which makes it easy to automate and implement [18]. Although EC treatment has been widely studied, most research has focused solely on removing pollutants without considering the remnant toxicity or secondary contamination by metal species added during treatment [19–22]. Specifically, it has been reported that in the presence of chloride, the EC process can lead to secondary reactions that, despite enhancing the removal of organic pollutants, are undesirable because they generate highly toxic chlorine containing intermediates (Eqs. 7–10) [4,23].

$$2Cl^- \rightarrow Cl_2 + 2e^- \tag{7}$$

$$Cl_2 + H_2O \rightarrow HOCl + HCl \tag{8}$$

$$HOCl + 2Fe^{2+} \rightarrow 2Fe^{3+} + Cl^- + OH^- \tag{9}$$

$$Dye + Cl_2 \rightarrow OxidizedDye + 2Cl^- \tag{10}$$

Therefore, monitoring environmentally concerning parameters such as toxicity is crucial as complex matrices such as those in TIWW are unpredictable, and treatment can cause several problems, such as the generation of highly toxic byproducts. Granulated activated carbon (AC) adsorption has been reported as an effective alternative for removing several kinds of pollutants, including dyes [24], and reducing toxicity in post electro-chemically treated effluents [25,26]. Therefore, several studies have used it as a post-process step to control treated effluent, achieving further organic-matter reduction as well [7]. Although several works have studied the EC process coupled with activated carbon adsorption (EC/AC) [25], most of them dealt with synthetic lab-prepared samples [25]. It is important to study real industry effluents because such samples are unpredictable and more complex than synthetic ones. Moreover, though few works have studied EC/AC with the real effluents [10,11], no studies have been conducted on TIWW polluted with indigo dye, which is a vat type dye that is one of the most light-stable organic dyes. This characteristic explains its longevity as a colorant that not only is highly resistant to treatments but that can be degraded into highly toxic byproducts.

Therefore, this study aims to apply the EC/AC process for real TIWW polluted with indigo dye to achieve discharge conditions that are nontoxic and biodegradable and that fulfill Colombia's environmental regulations at the lowest possible cost. This is accomplished through an experimental design coupled with nonlinear optimization.

2. Materials and Methods

2.1. Sample handling

A sample of TIWW was collected from a homogenization tank at the end of the manufacturing process at a textile plant in Medellin, Colombia. The sample was stored at 4 °C to prevent self-degradation. An initial characterization of the sample was performed to serve as a baseline for comparison of post-treatment sample parameters. Additionally, periodic measures of chemical oxygen demand (COD), total organic carbon (TOC), and absorbance (660 nm) were performed as indicators that the sample did not change significantly over time.

2.2. Characterization methods

Different parameters were measured in duplicate to characterize the samples using an ultraviolet-visible (UV-vis) double-beam spectrophotometer (Spectronic Genesys 2PC) following the standard methods of the American Public Health Association [27]. The UV-vis spectrum was measured in the 200–700 nm range to monitor the behavior of organic aromatic pollutants. Moreover, absorbance at 660 nm and true coloration (TC) (ISO 7887: 2011) served as indicators of the sample's blue coloration. COD (method 5220D) and TOC (method 5310D) were measured as indicators of organic pollutant content in the sample. Biodegradability was assessed by using the proportion of biological oxygen demand over 5 days (BOD_5) (method 5210B) relative to COD over a 5 day time frame, and toxicity was assessed by checking the mortality of *Artemia salina* when exposed to the sample following the method used by Manfra et al. [28]. Further, turbidity (method 2130B) and total solids (2540B) were measured as indicators of sample quality. We determined the Cl^- content using the standard Volhard titrimetric argentometry method and found it to be 625 mg/L.

2.3. Toxicity measurement

As it is known that the EC process may increase the toxicity of wastewater, the sample was tested for toxicity following the method used by Da Costa Filho et al. [29], which measures toxicity by exposing *A. salina* crustaceans to the sample for 24 hours. The *A. salina* were bred beforehand for 24 h in an aqueous growth medium with the necessary conditions for the survival of the subjects (35 g/L NaCl; lateral illumination of 3,500 lx; 25 °C). Test plates containing 20 *A. salina* crustaceans in 9.5 mL of sample solution and 0.5 mL of growth medium were then incubated for 24 h, with no nourishment provided between hatching and testing. The crustaceans were considered immobile if they remained still for 15 s during observation. Acute toxicity was calculated as the percentage of immobilization compared to a nontoxic control. The mortality of *A. salina* was calculated as follows:

$$Mortality\ (\%) = \left(\frac{\mathrm{N_o} - \mathrm{N_t}}{\mathrm{N_o}}\right) x100 \tag{11}$$

2.4. Biodegradability measurement

Biodegradability was measured using WTW Oxitop-C measuring heads and an Oxitop OC100 controller. To measure BOD, 1:1 dilutions of the sample were prepared in a WTW spectroquant BOD nutrient solution. We then followed the procedure described in ISO 5815 to measure BOD_5. Oxygen consumption was monitored by the measuring heads every 8 h and was compared to a control sample with no added microorganisms. The biodegradability index (BOD_5/COD ratio) has been extensively used in previous research as an indicator of wastewater biodegradability, and a threshold value greater than 0.35 is generally accepted as biodegradable [30–33].

2.5. Molecular weight distribution and analysis of after process pollutants

Molecular weight distribution (MWD) analysis of the sample after processing was used to better understand the nature of the pollutants after each phase of the process [34–37]. Ultrafiltration (UF) was performed in a 50-mL Amicon stirred-cell UF system (Millipore-Merck) with ultracell regenerated cellulose membranes of 44.5 mm (Millipore Corporation). This was performed to separate the pollutants based on their MWD (in cut-offs of 3, 5, 10, and 30 kDa). The membranes were stored in an 0.1 v/v ethanol-water solution at 4 °C, washed for 30 min with a 0.1 M NaOH solution, and then flushed with deionized water before usage, as instructed by the manufacturer. The operational UF pressure was kept constant at 0.4 MPa by a steady supply of nitrogen. The first 5 mL of filtrate for each membrane was discarded to avoid cross contamination due to membrane fouling. The color, COD, TOC, and toxicity for each filtrate were then measured to indicate the organic-matter concentration of each fraction.

2.6. EC process

The EC experiments were performed in a 100-mL borosilicate glass reactor containing TIWW at a temperature of 22 °C with a 60 rpm agitation to prevent floc formation. Iron electrodes (1.5 cm x 3.5 cm x 0.5 cm) were used as anode and cathode with a fixed submerged area and a gap of 1 cm between them so current density (*j*) could be controlled by changing the electric current. The aqueous phase's pH was controlled by adding H_2SO_4 (Merck; 98% purity) or 1 M NaOH solution as appropriate. Additionally, the process's conductivity (σ)was controlled by adding NaCl. The reaction time, pH, current density, and conductivity were set following the 4-factor Box-Behnken experimental design (BBD). After each run, the supernatant phase was filtered and centrifuged at 4000 rpm, then its COD, color, and turbidity were measured to determine the percentages of COD degradation (%DCOD), color degradation (%DC), and turbidity degradation (%DT), which served as response variables for the experimental design.

To assess the viability of the EC process, we considered operational cost (OC) as one of the response variables, and calculated this variable to be used as the optimization methodology's objective. The process OC was calculated as follows [11]:

$$OC\left[\frac{USD}{m^3}\right] = \frac{(I*V*t)*C_{kWh} + C_{pH} + \left(\frac{M*I*t}{z*F}\right)*C_{Fe} + C_s}{V} \tag{12}$$

where *I* and *V* are the electrical current and voltage used during process time t, respectively, C_{kWh} is the cost of electricity for the industrial sector by a local provider, C_{pH} is the cost of the H_2SO_4 or NaOH required to set the pH to the required condition, M is the molar mass of iron, z is the valency of iron in an ion form, F is the Faraday constant, C_{Fe} is the cost per kilogram of iron, and C_s is the cost of the treatment for the generated sludge. Lastly, V is the volume of the sample treated under such conditions.

2.7. Optimization process

We performed a linear regression to correlate the experimental results to the process variables. This was done by finding the parameters β_n of an empirical second-order model of the form:

$$Y_i = \beta_0 + \sum_{i=1}^{3} \beta_i x_i + \sum_{i=1}^{3} \beta_i x_i^2 + \sum_{i=1}^{3} \sum_{j=1}^{3} \beta_{ij} x_i x_j \tag{13}$$

where β_0, β_i, and β_{ij} are the regression parameters for input variables x_i and x_j. The model was achieved through multivariable regression using the R programming language [38,39], and the linear regression assumptions were checked and analysis of variance (ANOVA) was used to analyze the model's fitting based on the R^2, and adj-R^2. The F-test's p-value was used to determine the statistical significance of the model *(i.e. to determine if the findings in our sample are statistically corresponding to those of the population with a 95% confidence interval from the F distribution)*. The model was used to analyze the behavior of process outputs relative to operational variables. Additionally, response-surface plots were generated to illustrate the input variables' effects on the response variables, similar methodologies have been used in previous studies [15,16,32].

These models were then used to optimize the process with min OC as the objective in the acceptable region of pH, a, *j*, and time that maintain satisfactory %DCOD, %DC, and %DT values. This was accomplished by nonlinear convex optimization with the following restrictions:

$$minOC = \beta_{0OC} + \sum_{i=1}^{3} \beta_{iOC} x_i + \sum_{i=1}^{3} \beta_{iOC} x_i^2 + \sum_{i=1}^{3} \sum_{j=1}^{3} \beta_{ijOC} x_i x_j \tag{14}$$

$$DCOD = \beta_{0COD} + \sum_{i=1}^{3} \beta_{iCOD} x_i + \sum_{i=1}^{3} \beta_{iCOD} x_i^2 + \sum_{i=1}^{3} \sum_{j=1}^{3} \beta_{ijCOD} x_i x_j \tag{15}$$

$$DCOD \geq MinDCOD \tag{16}$$

where OC and DCOD are the OC and COD degradation, respectively, β_0, β_i, and β_{ij} are the OC and COD regression coefficients, and MinDCOD is the minimum acceptable COD degradation. Although the regression coefficients may be different for OC and DCOD, x_i and x_j are the same in both equations. Further, their values are restricted to the studied range. We used the fmincon function in Matlab to calculate the conditions that minimize OC while keeping DCOD higher than MinDCOD.

2.8. Activated carbon (AC) process

For the AC adsorption experiments, different amounts of AC (6, 10, 12, 16 and 20 g/L) were added to 100 mL of EC-treated samples (under optimum conditions), and the system was continuously stirred at 160 rpm for 4 h, at which time adsorption equilibrium was achieved. Other experimental conditions included a pH of 6.9 ± 0.1 and temperature of 26 °C ± 0.5 °C. The used AC was commercial coconut-based granular activated carbon (GAC) manufactured via high temperature steam activation (Hong-Yu, Taiwan) was used as received. The average physical properties of GAC were: total surface area (BET) = 1200 m^2/g, Iodine Number = 1150 mg/g, apparent density =482 kg/m^3, U.S. Standard Sieve Size (Mesh Size) 30 and Ash, Max (ASTM D-2866) 3

After the adsorption process, the sample was vacuum filtered, and the free and total chlorine concentrations were measured to quantify the amounts of adsorbed free and total chlorine. Additionally, DCOD, DC, DT, biodegradability, toxicity, and UV-vis spectrum were measured to determine the optimal AC dose and adsorption time.

OC_{AC} was also considered for this step as shown in Eq. (17), with the objective of minimizing the final effluent's toxicity at the lowest possible cost.

$$OC_{AC}\left[\frac{USD}{m^3}\right] = \frac{M_{AC} * C_{AC}}{V} \tag{17}$$

Here, M_{AC} is the mass of AC used during the adsorption and C_{AC} is the cost per mass unit of AC. The total cost of the process was thus calculated as the sum of the cost of OC and OC_{AC} (Eq. 18).

$$OC_{Total}\left[\frac{USD}{m^3}\right] = OC + OC_{AC} \tag{18}$$

3. Results and Discussion

3.1. Sample characterization

Table 1 presents the characteristics of the sample used for this study, and shows a parallel between these characteristics and Colombian emission limits. Additionally, the efficiency of both EC/AC treatment steps is presented. The TIWW presents a slightly acidic pH and high organic load, with 97% of the COD related to auxiliary products and only 3% to dyes. A high concentration of chloride ions (625 mg Cl^-/L) is also observed, which may be related to the high dose of NaCl that is often used as a retardant agent in reactive dyeing during the dyeing process. The TIWW UV-vis spectrum showed the maximum absorbance at 660 nm, corresponding mainly to the indigo dye, which is the main raw material in the denim dyeing process. The wastewater shows a greenish-blue color, equivalent to 1193 mg Pt-Co/L. Furthermore, very similar absorbance values were observed at 436 nm, 525 nm, and 620 nm, indicating the presence of violet, green, and orange in the wastewater absorption spectrum. Moreover, based on the low BOD_5/COD ratio (approximately 0.13), a low biodegradability was attributed to the raw industrial wastewater, which is in accordance with previous research on TIWW [7,40,41]. Notice that the raw sample's COD does not comply with regulations, whereas that of the post-EC sample does.

3.2. BBD experimental results: Model fit and statistical analysis

A BBD experiment was performed for the EC experimental runs [13,41]. In this experiment, pH, σ, *j*, and time were selected as

Table 1
Characterization of textile industrial wastewater (TIWW) before and after electrocoagulation (EC) and activated carbon (AC) treatment, and efficiency under optimal operating conditions.

Parameter	TIWW	EC	Treatment Efficiency (%)	EC/AC	Overall Efficiency (%)
pH	6.0	7	-	8	-
Conductivity (mS/cm)	2.5	2.4	-	2.2	-
Turbidity (NTU)	206	10	95	6	97
COD (mg O_2/L)	840	311	63	235	72
TOC (mg O_2/L)	215	105	51	85	60.5
BOD_5 (mg O_2/L)	107.2	74.5	31	61	43
Total solids (g/L)	3.4	0.4	88	0.32	91
Chloride - Cl^- (mg/L)	625	595	4.8	590	5.6
AOX (mg/L) photometric method (985007) Machery-Nagel	16.5	9.6	42	3.2	81
Total chlorine (mg/L) photometric method (91816) Machery-Nagel	15.6	40	-	3.7	91
Absorbance (660 nm)	1.11	0.03	97	0.02	98
True Color ISO 7887:2012-04 (B)	λ_{436} = 72.4 λ_{525} = 61.6 λ_{620} = 71.3	λ_{436} = 3.3 λ_{525} = 2.0 λ_{620} =1.6	95 (λ_{436}) 97 (λ_{525}) 98 (λ_{620})	λ_{436} = 3.1 λ_{525} = 2.0 λ_{620} = 1.3	96 (λ_{436}) 97 (λ_{525}) 98 (λ_{620})
ISO 7887 Method C mg/$L_{Pt\text{-}Co}$	1,193	60	95	48	96
BOD_5/COD	0.13	0.24	-	0.29	-
Toxicity	100	45	55	0	100
Generated sludge (kg/m^3)		0.35		0.35	
OC_{Total} (USD/m^3)	-	0.92		1.1	

Table 2
Experimental results of the electrocoagulation process for chemical oxygen demand degradation (%DCOD), color degradation (%DC), turbidity degradation (%DT), and organic carbon based on the Box-Behnken experimental design (BBD).

pH	σ (mS/cm)	*j* (mA/cm^2)	t (min)	%DCOD	%DC	%DT	OC (USD/m^3)	V
6	3	10	10	54	92	95	0.766	6.3
3	2	10	10	53	90	94	0.975	4.5
9	2	10	10	54	83	91	0.822	4.9
3	4	10	10	52	88	66	1.036	5.4
9	4	10	10	66	92	93	0.876	5.7
6	3	5	5	44	70	62	0.215	5.1
6	3	15	5	52	88	91	0.501	5.7
6	3	5	15	33	92	90	0.584	3.9
6	3	15	15	67	88	95	1.713	7.1
3	3	10	5	50	69	62	0.639	4.1
9	3	10	5	55	82	82	0.483	4.8
3	3	10	15	54	92	85	1.358	5.1
9	3	10	15	60	85	91	1.168	5.0
6	3	10	10	56	91	92	0.685	5.1
6	2	5	10	34	90	95	0.386	3.8
6	4	5	10	49	90	74	0.416	4.7
6	2	15	10	61	86	94	1.162	7.3
6	4	15	10	68	95	95	1.072	6.4
3	3	5	10	33	87	88	0.740	4.5
9	3	5	10	50	88	84	0.549	4.2
3	3	15	10	62	89	82	1.482	7.2
9	3	15	10	64	92	94	1.312	7.3
6	2	10	5	50	82	85	0.369	5.9
6	4	10	5	58	81	57	0.369	5.9
6	2	10	15	57	84	91	1.058	5.4
6	4	10	15	62	93	84	1.098	5.8
6	3	10	10	52	90	92	0.779	6.5

independent variables, and %DC, %DCOD, %DT, and OC were chosen as response variables. Table 2 shows the experimental runs and results of the BBD.

Experimental data for each of the response variables was fitted to a quadratic model of the independent variables by multivariate linear regression analysis using R. The ANOVA for the models is presented in Table 3. The R^2 and $R_{Adj\text{-}}$ values indicate the level at which the model explains the variability in the data, with respective values of 0.97 and 0.94 for %DCOD, 0.94 and 0.87 for %DC, 0.93 and 0.85 for DT, and 0.99 and 0.98 for OC, indicating that the model can effectively explain variability in the dataset [32,38]. Additionally, the F-test indicates that the model provides a better fit than the intercept-only model (i.e., the model is significant). This is shown by p-values of almost 0 for all of the models, which are below the significance level of 0.05, indicating that all of the models are significant. ANOVA also shows p-values for the independent variables and interactions, with p-values of less than 0.05 indicating that the model with the respective variable provides a better fit than the model without it (i.e., the variable is significant) [38]. Therefore, as shown in Table 3, the considered variables are all significant toward most of the response variables and thus shall be included in the quadratic models shown in Eqs. (19)–(22).

$$\begin{aligned} COD = {} & 33.1 - 0.94*pH - 11.16*\sigma + 5.11*j - 1.51*t + 0.11*pH^2 \\ & + 1.08*pH*\sigma - 0.25*pH*j + 0.016*pH*t + 2.33*\sigma^2 \\ & - 0.4*\sigma*j - 0.15*\sigma*t - 0.14*j^2 + 0.26*j*t - 0.016*t^2 \end{aligned} \tag{19}$$

$$\begin{aligned} DC = {} & 37.5 + 3.61*pH - 11.5*\sigma + 1.11*j + 8.73*t - 0.26*pH^2 \\ & + 0.92*pH*\sigma + 0.03*pH*j - 0.33*pH*t - 0.25*\sigma^2 \\ & + 0.45*\sigma*j + 0.5*\sigma*t - 0.005*j^2 - 0.22*j*t - 0.25*t^2 \end{aligned} \tag{20}$$

$$\begin{aligned} DT = {} & 78.75 - 0.38*pH - 22.25*\sigma + 1.23*j + 9.4*t - 0.48*pH^2 \\ & + 2.5*pH*\sigma + 0.26*pH*j - 0.23*pH*t - 3.5*\sigma^2 + 1.11*\sigma*j \\ & + 1.05*\sigma*t - 0.015*j^2 - 0.24*j*t - 0.36*t^2 \end{aligned} \tag{21}$$

$$\begin{aligned} OC = {} & 0.9 - 0.3*pH + 0.14*\sigma - 0.032*j - 0.0097*t + 0.023*pH^2 \\ & + 0.002*j^2 + 0.008*j*t \end{aligned} \tag{22}$$

The Breusch-Pagan test yielded p-values of 0.46, 0.09, 0.08, and 0.67 for DCOD, DC, DT, and OC, respectively. This indicates the homoscedasticity of residuals in these models, thus fulfilling the linear regression assumption [32]. However, it's also clear that DCOD and OC comply with the linear regression assumptions better than the others, and DC and DT are generally at a level that complies with the regulation; therefore, the former were used for optimization.

3.3. Optimization and effects of process variables

Nonlinear programming was used to determine the best process variable conditions based on the obtained quadratic models. The fmincon function in the Matlab environment was used to minimize OC while maintaining a %DCOD of at least 60% as a constraint. It was

Table 3
Analysis of variance for %DC, %DCOD, %DT, and OC as a function of initial pH, σ,*j*, and time.

	%DCOD					%DC				
Variable	Df	Sum Sq	Mean Sq	F value	p-value	Df	Sum Sq	Mean Sq	F value	p-value
pH	1.00	168.75	168.75	35.89	0.00	1.00	4.08	4.08	0.86	0.37
σ	1.00	176.33	176.33	37.51	0.00	1.00	48.00	48.00	10.09	0.01
j	1.00	1430.08	1430.08	304.18	0.00	1.00	36.75	36.75	7.73	0.02
t	1.00	48.00	48.00	10.21	0.01	1.00	320.33	320.33	67.34	0.00
pH^2	1.00	10.98	10.98	2.34	0.15	1.00	7.35	7.35	1.55	0.24
σ^2	1.00	70.67	70.67	15.03	0.00	1.00	11.56	11.56	2.43	0.15
j^2	1.00	69.47	69.47	14.78	0.00	1.00	23.01	23.01	4.84	0.05
t^2	1.00	0.93	0.93	0.20	0.67	1.00	208.33	208.33	43.80	0.00
pH:σ	1.00	42.25	42.25	8.99	0.01	1.00	30.25	30.25	6.36	0.03
pH:j	1.00	56.25	56.25	11.96	0.00	1.00	1.00	1.00	0.21	0.65
pH:t	1.00	0.25	0.25	0.05	0.82	1.00	100.00	100.00	21.02	0.00
σ:j	1.00	16.00	16.00	3.40	0.09	1.00	20.25	20.25	4.26	0.06
σ:t	1.00	2.25	2.25	0.48	0.50	1.00	25.00	25.00	5.26	0.04
j:t	1.00	169.00	169.00	35.95	0.00	1.00	121.00	121.00	25.44	0.00
Residuals	12.00	56.42	4.70	NA	NA	12.00	57.08	4.76	NA	NA
	R^2	R^2_{adj}	Residual St-Er	F stat	p-val	R^2	R^2_{adj}	Residual St-Er	F stati	p-value
Model	0.97	0.94	2.16	34.35	1.69E-07	0.94	0.87	2.18	14.37	2.19E-05
	OC					%DT				
Variable	Df	Sum Sq	Mean Sq	F value	p-value	Df	Sum Sq	Mean Sq	F value	p-value
pH	1.00	0.09	0.09	48.03	0.00	1.00	280.33	280.33	15.59	0.00
σ	1.00	0.00	0.00	0.40	0.54	1.00	546.75	546.75	30.41	0.00
j	1.00	1.58	1.58	874.24	0.00	1.00	280.33	280.33	15.59	0.00
t	1.00	0.94	0.94	521.89	0.00	1.00	784.08	784.08	43.61	0.00
pH^2	1.00	0.29	0.29	160.39	0.00	1.00	21.60	21.60	1.20	0.29
σ^2	1.00	0.00	0.00	1.53	0.24	1.00	8.56	8.56	0.48	0.50
j^2	1.00	0.02	0.02	9.77	0.01	1.00	41.34	41.34	2.30	0.16
t^2	1.00	0.00	0.00	2.07	0.18	1.00	432.00	432.00	24.03	0.00
pH:σ	1.00	0.00	0.00	0.01	0.94	1.00	225.00	225.00	12.51	0.00
pH:*j*	1.00	0.00	0.00	0.06	0.82	1.00	64.00	64.00	3.56	0.08
pH:t	1.00	0.00	0.00	0.15	0.70	1.00	49.00	49.00	2.73	0.12
σ:*j*	1.00	0.00	0.00	2.01	0.18	1.00	121.00	121.00	6.73	0.02
σ:t	1.00	0.00	0.00	0.22	0.65	1.00	110.25	110.25	6.13	0.03
j:t	1.00	0.18	0.18	98.38	0.00	1.00	144.00	144.00	8.01	0.02
Residuals	12.00	0.02	0.00	NA	NA	12.00	215.75	17.98	NA	NA
	R^2	R^2_{adj}	Residual St-Er	F stat	p-value	R^2	R^2_{adj}	Residual St-Er	F stat	p-value
Model	0.99	0.98	0.042	122.8	9.891E-11	0.93	0.85	4.24	12.35	4.91E-05

found that a pH = 5.4, σ = 2 mS/cm, j = 14 mA/cm^2, and t = 11 min yielded the optimum cost for the system in the studied range, which was 0.92 USD/m^3 with 62% DCOD. Fig. 1 shows the three-dimensional response surfaces generated from Eqs. (19–22) for the different response variables. These response surfaces show the behavior of two variables when the rest are fixed at optimum conditions.

3.3.1. Effect of conductivity (σ)

Conductivity in the sample has two major effects on the system. First, higher conductivity leads to a lower cell potency (i.e., lower energy consumption), which also leads to a decrease in the OC of the process that surpasses the cost of the electrolyte itself, as shown in Fig. 1a. The second effect is that a higher conductivity indicates a higher number of electrolytes that can react on the anode to form oxidizing species, such as HOCl and ClO^- in the case of NaCl as shown in Eq. (8), which exist in equilibrium depending on the treated sample's pH [4,40]. These species favor the degradation of organic pollutants, but also lead to the formation of organo-chlorinated components increasing toxicity. Because toxicity is to be avoided and because the objective is not to maximize DCOD but rather to minimize OC, the extra DCOD provided by chlorine species is unnecessary and the optimum σ = 2 mS/cm seems acceptable. Nippatla et al. [40] evaluated conductivity's effects on the EC process for textile dyes in the range between 2 and 8 mS/cm, and obtained the highest degradation at the higher level; however, the process wasn't optimized and toxicity due to the generation of Cl species was not considered.

3.3.2. Effect of pH

The effect of pH in the EC process is mainly related to iron coagulant species in the solution, which exist in equilibrium and prevail depending on the pH. This affects the process because different species yield varying coagulation performances for different pollutants[8]. The effect of pH can also be attributed to changes in the physico-chemical behavior of the pollutants as a function of pH [4]. It has been reported that neutral to slightly acidic media show better EC performance, matching the experimental results (optimum pH = 5.4) as shown in Fig. 1 (a, b, and c); however, the opposite effect occurs at high conductivity values, probably because the nature of chlorine species generated at the anode vary with different pH conditions, enhancing or hindering the process. Moreover, during the EC process, a sudden pH variation was observed. If the initial pH value was 3 (acidic medium), the final pH of the treated effluent was around 6.8 to 7.0, and when the initial pH value was 6, the final value was between 7 and 7.4. However, pH decreased between 1 and 0.7 units when the initial pH value was (alkaline medium). Similar results were described by Hendaoui et al. [8] and Varank et al [42]. This behavior can be attributed to the formation of H_2 gas and release OH^- during the EC and the generation HClO [4].

3.3.3. Effect of current density (j)

Current density controls the reactions that occur in solution as well as their kinetics [13,40], and is the major source of OC in the process. The application of a higher j value may lead a greater electrodissolution of iron ions and electrogeneration of oxidant Cl species and, as a consequence, a higher DCOD, as can be seen in Fig. 1 (b–f); However, as j is the main source of OC, lowering j values is likely to be one of the main objectives for the optimization algorithm to yield the maximum treatment performance with the lowest possible cost. This matches the

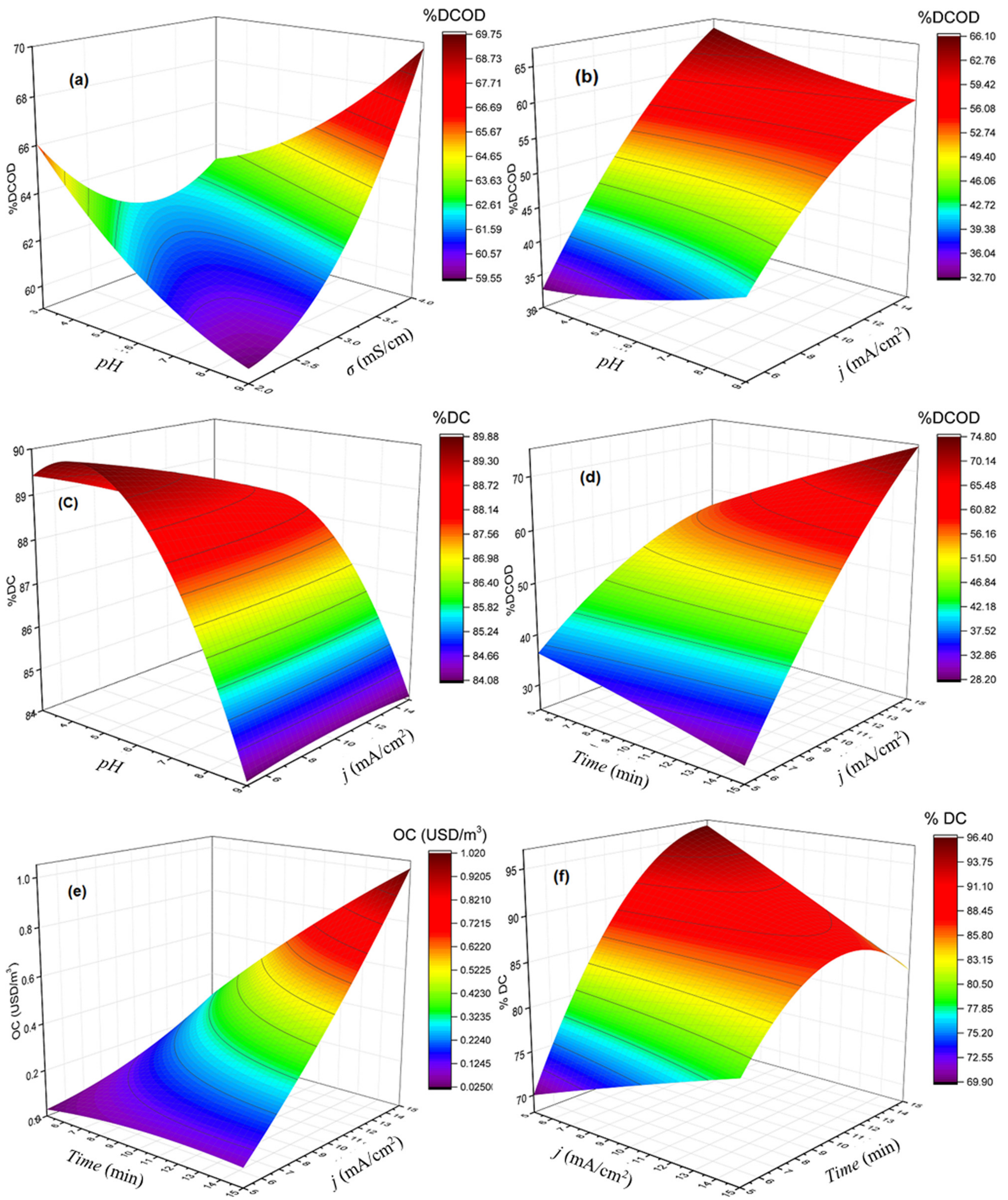

Fig. 1. Three-dimensional response surfaces generated from the BBD method using Eqs. (19,20, and 22) for DC, DCOD, and OC.

results reported by Verma [3], who also worked with TIWW and reported that color and %COD tend to stabilize after 15 mA/cm^2.

3.3.4. Effect of time

Because pH, σ, and *j* affect the kinetics of iron electrodissolution, and coagulant and oxidizing species generation, it is expected that the time covariant interacts with all of them [11,13]. In general, as only suspended matter can be coagulated, EC performance reaches a plateau when all the suspended matter has been removed. However, Fig. 1 (e and f) show that when *j* is low, an increase in time would lead to decreased DCOD, likely because of the destabilization of coagulant particles. In contrast, the opposite happens at when *j* is high, where DCOD kept increasing in the studied range, probably because of the generation of oxidant chlorine species. However, DC started decreasing because the solution tends to become yellowish with the excess release of iron ions.

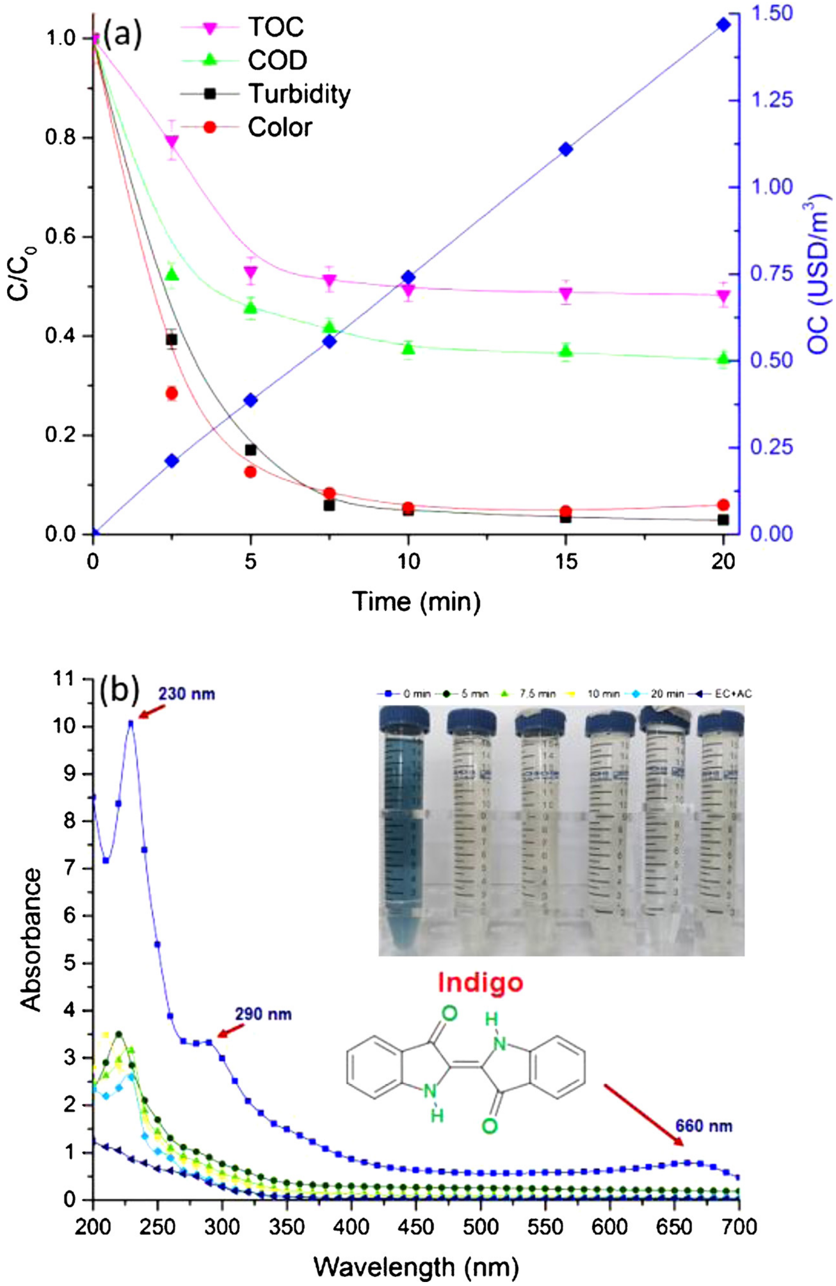

Fig. 2. Organic-matter removal during 20 min of the EC process under optimal conditions (pH = 5.4, σ = 2 mS/cm, and j = 14 mA/cm^2). (a) COD, TOC, color, and OC; (b) UV-vis spectrum. The error bars indicate the variance of the data.

Time plays a major role in process cost as using a cell potency for longer times leads to higher costs [3,11,12,40]. Based on the results of the optimization algorithm, maximum efficiency is obtained at minute 11, as this is the minimum time required for the process to achieve the necessary degradation. This result is lower than that reported by other authors, such as Khorram and Fallah [13], who optimized the time of decolorization for TIWW by the EC process and reported a minimum time of approximately 23 min for 98% decolorization and 40% COD removal. These differences can be attributed to the varying characteristics of real TIWW.

3.3.5. Analysis of during and after process variables

Color, COD, TOC, turbidity, and OC were monitored during the EC process over time to better understand their behavior and verify the information the models provided. Fig. 2 shows that color was almost completely removed a few minutes after the process started, whereas COD and TOC reached a plateau at around 55% and 50%, respectively, within approximately 10 minutes of reaction time. This is because EC mainly removes suspended organic matter [37,41] and leaves a dissolved remnant in the sample that corresponds with the remaining COD and TOC.

Furthermore, the kinetic study was performed based on the removal of COD and TOC evaluated under optimal conditions as described by the following equation [11]:

$$\frac{dC_t}{dt} = k * C^n \tag{23}$$

For the pseudo-zero, pseudo-first, and pseudo-second-order kinetics, the value of reaction order (n) is equal to 0, 1, and 2, respectively. By replacing the value of n for each of the mentioned reaction orders into Eq. (23) and integrating it, the following equations were obtained for the zero, first, and second-order kinetics, respectively:

$$C_t = C_0 - k_0 * t \tag{24}$$

$$Ln\left(\frac{C_0}{C_t}\right) = k_1 * t \tag{25}$$

$$\frac{1}{C_t} - \frac{1}{C_0} = k_2 * t \tag{26}$$

where C_o is the initial concentration (COD or TOC); C_t is the concentration at time t; and k_0 (mg/L-min), k_1 (min^{-1}), and k_2 (L/mg-min) are the zero, first, and second-order reaction rate constants, respectively. The plots of C_t/C_0 vs. time (for n = 0), ln (C_0/C_t) vs. time (for n = 1), and ((1/C_t) -(1/C_0)) vs. time (for n = 2) should exhibit linear tendencies for each order of reaction (n). Therefore, to select an adequate reaction order, one must determine which transformation is better fitted by a linear regression. The three models have very high R^2 and Adj-R^2 values; therefore, a different parameter, such as the Akaike information criterion (AIC), which is an objective parameter quantifying the suitability of a particular model relative to a set of models [31,43], can be used. A lower AIC value suggests that the model fits the data better, is less complex, or a combination of both. Based on the obtained results, the EC performance proved to be well-described by the second-order kinetics. The values of k were calculated by applying a least square regression analysis, and the results are shown in Fig. 3. Similar fits of second-order kinetics were obtained by Bener et al. [11] and Amani-Ghadim et al. [44].

Analyzing the data of the process over time not only served to better understand the behavior of different parameters during the EC process, it also served to verify the regression model. In summary, the experimental results shown in Fig. 2 show that the EC process under the optimum conditions of pH = 5.4, σ =2 mS/cm, and$j$ =14 mA/cm^2, achieved %DC, %DT, %COD, and %TOC values of 95%, 95%, 63%, and 51%, respectively, with approximately 10 minutes of reaction time. This matches the results obtained through the optimization algorithm. Additionally, the process adjusted to a pseudo-second order kinetic model with $k_2 = 5.5*10^{-4}$ for COD and $k_2 = 2.1*10^{-4}$ for TOC. These results differ from those observed by Bener et al., who applied the EC process with aluminum electrodes to deal with TIWW and found that j =25 mA/cm^2, σ =7.4 mS/cm, pH = 5, and t=120 min would lead to %DC, %DT, %COD, and %TOC values of 95%, 83.5%, 18.6%, and 65%, respectively, at a cost of 1.5 USD/m^3. These differences are likely due to the focus of the optimization approach in that study being maximizing %TOC, one variable at a time, rather than minimizing cost with an optimization algorithm, thus achieving a greater degradation at a higher j and higher cost.

In contrast, the pollutants in industrial textile effluents include organic and inorganic products such as finishing agents, surfactants, inhibitor compounds, active substances, chlorine compounds, salts, dyeing substances, total phosphate, dissolved solids, and total suspended solids [2,40,45]. In the EC process, the use of NaCl as electrolyte can lead to anodic oxidation of Cl to produce chlorine species like Cl_2, HClO, and ClO_6, which can oxidize organic materials [46–48]. Nevertheless, degradation with said species may lead to important disadvantages [1] such as (i) the formation of undesirable toxic chloro-organic derivatives and (ii) the electrogeneration of chlorine-oxygen byproducts such as chlorite, chlorate, and perchlorate (as shown in Eqs. (7)–(10)), which pose high health risks. As a consequence, chlorine and intermediates should be removed before discharge.

Consequently, the toxicity in the sample after EC was monitored. The toxicity of the initial sample was 100% and decreased to 45% after the EC process, with the remaining toxicity being attributed to either the initial toxicity of the dissolved components or the generation of toxic compounds by process reactions. Therefore, activated carbon was used to remove the toxicity of waters treated by EC.

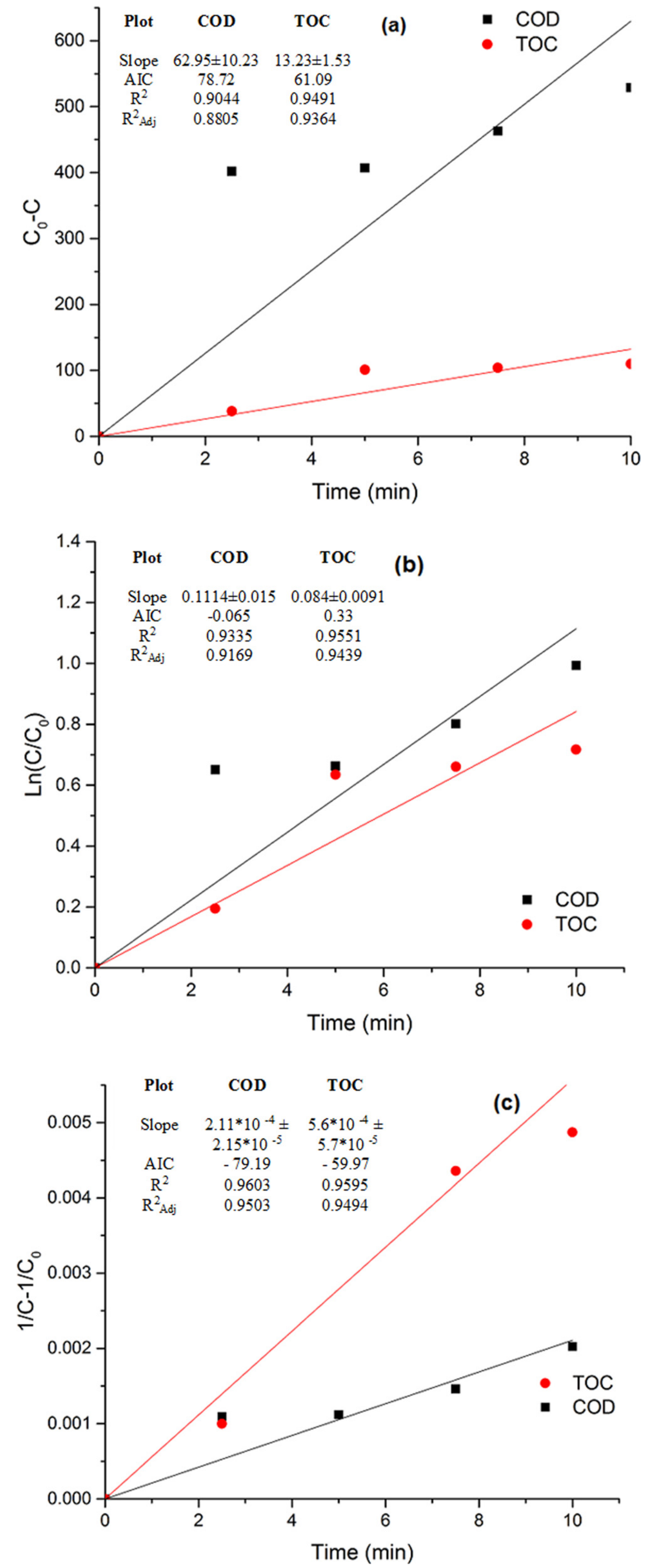

Fig. 3. (a) Pseudo-zero, (b) pseudo-first, and (c) pseudo-second-order models for COD and TOC in the EC process under optimum conditions (pH = 5.4, σ =2 mS/cm, j =14 mA/cm^2). k = 62, 0.11, and $5.5*10^{-4}$ in the pseudo-zero, first. and second-order models, respectively, for COD; and 13.2, 0.08, and $2.1*10^{-4}$ in the respective models for TOC.

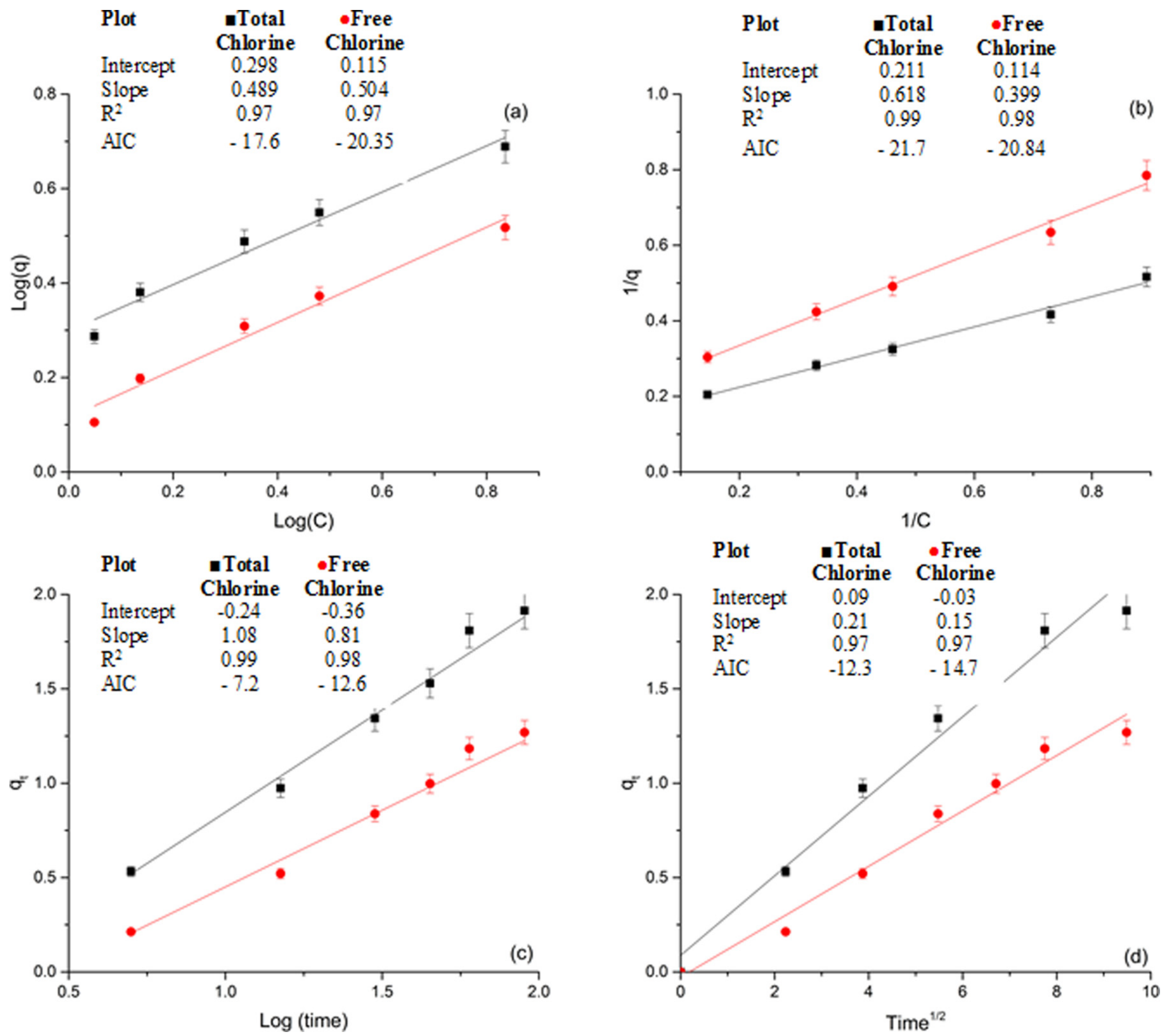

Fig. 4. Adsorption isotherms and kinetics for free and total Cl adsorption on AC. (a) Freundlich isotherm, (b) Langmuir Isotherm, (c) Elovich kinetics, and (d) Weber-Morris kinetics.

3.4. AC adsorption

AC is ideal for removing active chlorine species from wastewater because it does not require the addition of reactants and can remove most persistent organic pollutants at the same time [41,49]. Adsorption isotherms indicate how adsorption molecules are distributed between the liquid and solid phases when the adsorption process has reached equilibrium. The analysis of isotherm data fitted to different isotherm models is an important step to finding a suitable model that can be used for design purposes [50]. We fitted adsorption isotherms to the Langmuir and Freundlich isotherm models, and the results are presented in Fig. 4. Furthermore, adsorption is a complex process, so it is imperative to understand its kinetics as they can be used to calculate the rate at which a pollutant is removed. This allows the optimization of variables to maximize the adsorption of free and total chlorine onto AC. Additionally, adsorption kinetics provide valuable data for understanding the involved mechanisms. Therefore, the experimental kinetic data were fitted by linear regression using the Weber-Morris and Elovich models. The linear regression results are also shown in Fig. 4.

The fittings of different isotherm and kinetic models to the adsorption data were compared by R^2 and AIC values, and these criteria are presented for each model in Fig. 4 (i.e., the values of the correlation coefficients (RR) for the Weber-Morris and Elovich models were higher than those of the pseudo-first and pseudo-second-order models). Although all of the presented models yielded acceptable R^2 and AIC values, the Langmuir isotherm (Fig. 4b) has AIC values of -21.96 and -20.84 for free and total chlorine, respectively, which are lower than the -17.6 and -20.35 obtained by the Freundlich isotherm (Fig. 4a). Therefore, we can conclude that the Langmuir isotherm is the most appropriate representation of the distribution of chlorine between the liquid and solid phases in the system's equilibrium. By a similar argument, we concluded that the Weber-Morris model (Fig. 4d) is the one that best described the AC adsorption kinetic as its AIC values were -12.27 and -14.74 for free and total chlorine, respectively, which are lower than those of the Elovich model (Fig. 4c).

The Langmuir isotherm was then used to determine the optimum quantity of AC to maximize Cl adsorption. The mass of adsorbed pollutants per unit of AC used stabilized at approximately 20 g/L of AC, which suggests that it is reasonable to select such an AC load for the process. The sample after EC was subjected to a 4 h AC adsorption experimental run at room temperature with 20 g/L of AC, and samples were taken every 15 min to understand the behavior of the real sample during the process. The results of this run are shown in Fig. 5. Although the organic matter was only slightly reduced, toxicity was null after the first hour of the AC process. Therefore, it seems reasonable to select 1 h as the time for the AC phase. Moreover, because AC can be reused several times, using AC adsorption as an additional step only increases the overall process cost (OC_{Total}) from 0.9 USD/m^3 to 1.1 USD/m^3, including the reactivation cost for AC. The overall EC/AC process led to a nontoxic sample with %DC, %COD, and %TOC values of 96%, 72%,

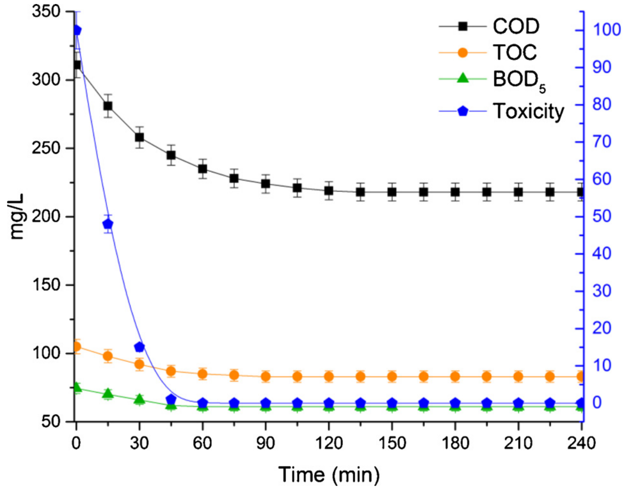

Fig. 5. Organic-matter removal and toxicity behavior after EC during 4 h of the AC process at room temperature with 20 g/L of AC and pH = 7.

and 60%, respectively. Chang et al. [25], reported a similar behavior for the EC/AC process when removing Reactive Black 5 (RB5) dye in a synthetic sample. The EC process showed high decolorization (100%) of the sample within 8 min of reaction at pH = 7, j = 27.7 mA/cm^2, and 1 g/L NaCl. However, there was a 61% COD remnant after the treatment and toxicity was high (97% light inhibition). The AC step using 20 g/L completely removed the toxicity, matching our results. However, they also reported a higher COD adsorption of up to 97% for the overall process, which is probably due to using a synthetic sample containing only RB5, which can be adsorbed on the AC surface.

Although the EC/AC process was able to remove 72% of COD and 60% of TOC, it is clear that there is an organic remnant in the after process sample. Fig. 6 shows the distribution profiles of color, COD, TOC, and toxicity for initial and post-process TIWW. The initial TIWW (Fig. 6a) was mainly colored by compounds in the > 30 kDa range, which yielded between 68% and 90% of the sample color depending on the measuring wavelength. This changed for the after process sample (Fig. 6b) where pollutants in the < 5 kDa range yielded approximately 60% of the color for each wavelength. A similar behavior was observed for COD and TOC, for which the initial TIWW was mainly polluted with organic pollutants in the > 30 kDa and < 3 kDa MW fractions, for which approximately 40% of COD and TOC can be attributed to the former (probably due to auxiliary chemicals such as surfactants, starch, waxes, oils, stabilizers, organic compounds, resins, carboxymethyl cellulose, etc.), and 43% of the organic matter can be attributed to the latter (due to the presence of formaldehyde and acids such as acetic acid, formic acid, and oxalic acid etc.). After the EC/AC process, not only were the COD and TOC concentrations significantly decreased, the profile changed, with approximately 80% of the COD and TOC classified in the < 3 kDa fraction and less than 10% found to be < 30 kDa. It has been pointed out that polymers and organics with MW > 30 kDa tend to be more biorecalcitrant than smaller and more soluble molecules because of the difficulty in gaining access inside bacterial cells [36,51]. This likely explains the overall increase in biodegradability after EC/AC. In contrast, Fig. 6a shows that most of the toxicity is also yielded by pollutants with higher MW, likely because the EC/AC process mainly removed these components, as well as any electro-chlorinated intermediaries. Thus, the toxicity was completely removed by the process, as shown in Fig. 6b.

The MWD evaluation showed that the EC/AC process is very effective in removing most large and complicated molecular structures. It has been shown that the EC process is not effective at removing compounds with MW < 5 kDa [34,36,41]. However, although most of the TOC removal can be attributed to the coagulation of bigger molecules, further degradation of the smaller molecules can be attributed to the generation of oxidant species and AC adsorption. However, these effects pale in comparison to the coagulation effect [4].

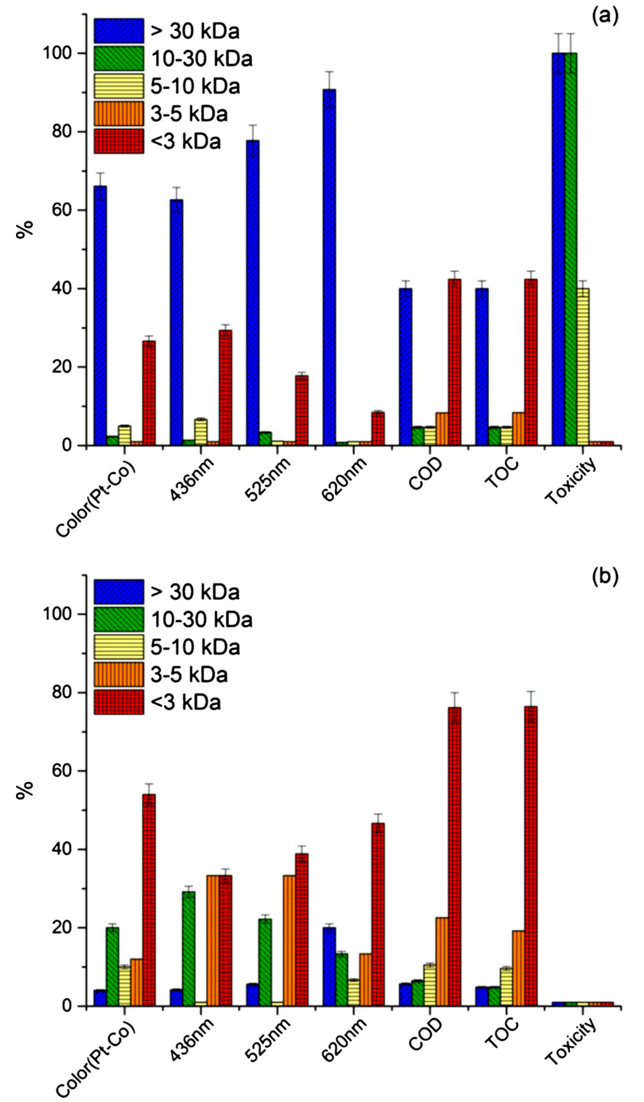

Fig. 6. Molecular weight distribution (MWD) of (a) raw TIWW and (b) TIWW after EC/AC treatment under optimal conditions (pH = 5.4, σ = 2 mS/cm, j = 14 mA/cm^2, and time = 11 min).

4. Conclusions

The results of this study show that the EC/AC process is effective for degrading TIWW effluents that contain persistent non-biodegradable pollutants. Linear regression and nonlinear optimization with constraints led to the lowest possible cost while keeping a high enough removal for discharge. These conditions were: pH = 5.4, σ = 2 mS/cm, j = 15 mA/cm^2, and t = 11 min to obtain color, COD, and TOC reductions of 95%, 63%, and 51%, respectively. However, the effluent showed remaining toxicity of 45%, which was removed using an AC adsorption process. The conditions for the AC adsorption process were determined using the Langmuir isotherm, and found to be a concentration of 20 g/L and duration of 1 h.

The whole EC/AC process led to reductions of 72% for COD, 60% for TOC, and 96% for color, toxicity was null and the biodegradability index (BOD_5/COD) increased from 0.13 to 0.29, suggesting that the effluent is acceptable for discharge. Further characterization showed that most of the toxicity is generated by the larger pollutants, which are quickly removed by the EC process, remaining toxicity is probably attributed to the electro-generated chlorinated compounds, which are removed by the AC step.

The total operative cost (OC_{Total}) of the AC/EC process was approximately 1.1 USD/m^3, which is similar the findings of other studies [4,8], while also controlling the toxicity issue. Moreover, this seems to be a technologically viable option as the EC/AC process can be operated in a continuous system and cost could be reduced further based on the reuse approach implemented for AC adsorption.

Author declaration

We confirm that the manuscript has been read and approved by all named authors and that there are no other persons who satisfied the criteria for authorship but are not listed. We further confirm that the order of authors listed in the manuscript has been approved by all of us.

Declaration of Competing Interest

There are no known conflicts of interest.

Acknowledgments

This article is published as a part of a research project supported by the Direction de Investigation de la Universidad EAFIT. The authors are grateful to the Universidad EAFIT for the financial support, and to the staff of the Laboratorio de Ingenieria de Procesos for their assistance.

References

[1] E. Brillas, C.A. Martinez-Huitle, Decontamination of wastewaters containing synthetic organic dyes by electrochemical methods, An updated review, Applied Catalysis B: Environmental 166-167 (2015) 603–643.
[2] B. Khemila, B. Merzouk, A. Chouder, R. Zidelkhir, J.-p. Leclerc, F. Lapicque, Removal of a textile dye using photovoltaic electroco-agulation, Sustainable Chemistry and Pharmacy 7 (2018) 27–35.
[3] A. Verma Kumar, Treatment of textile wastewaters by electrocoagu-lation employing Fe-Al composite electrode, Journal of Water Process Engineering 20 (2017) 168–172.
[4] S. Garcia-Segura, M. Maesia, S.G. Eiband, J. Vieira, D. Melo, C.A. Martinez-Huitle, Electrocoagulation and advanced electrocoagulation processes: A general review about the fundamentals, emerging applications and its association with other technologies, Journal of Electro-analytical Chemistry 801 (2017) 267–299.
[5] H. Zazou, H. Afanga, S. Akhouairi, H. Ouchtak, A. Ait Addi, R. Ait Akbour, A. Assabbane, J. Douch, A. Elmchaouri, J. Duplay, A. Jada, M. Hamdani, Treatment of textile industry wastewater by electrocoagulation coupled with electrochemical advanced oxidation process, Journal of Water Process Engineering 28 (2019) 214–221.
[6] O. Tunay, M. Imeker, N. Kabdal, T. Olmez-Hanci, Abatements of reduced sulphur compounds, colour, and organic matter from indigo dyeing effluents by electrocoagulation, Environmental Technology 35 (2014) 1577–1588.
[7] E. GilPavas, I. Dobrosz-Giomez, M.A. Giomez-Garcia, Optimization of sequential chemical coagulation - electro-oxidation process for the treatment of an industrial textile wastewater, Journal of Water Process Engineering 22 (2018) 73–79.
[8] K. Hendaoui, F. Ayari, I.B. Rayana, R.B. Amar, F. Darragi, M. Trabelsi-Ayadi, Real indigo dyeing effluent decontamination using continuous electrocoagulation cell: Study and optimization using response surface methodology, Process Safety and Environmental Protection 116 (2018) 578–589.
[9] M. Oncel, A. Muhcu, E. Demirbas, M. Kobya, A comparative study of chemical precipitation and electrocoagulation for treatment of coal acid drainage wastewater, Journal of Environmental Chemical Engineering 1 (2013) 989–995.
[10] J. Nunez, M. Yeber, N. Cisternas, R. Thibaut, P. Medina, C. Carrasco, Application of electrocoagulation for the efficient pollutants removal to reuse the treated wastewater in the dyeing process of the textile industry, Journal of Hazardous Materials 371 (2019) 705–711.
[11] S. Bener, O. Bulca, B. Palas, G. Tekin, S. Atalay, G. Ersoz, Electrocoagulation process for the treatment of real textile wastewater : Effect of operative conditions on the organic carbon removal and kinetic study, Process Safety and Environmental Protection 129 (2019) 47–54.
[12] L. Bilinska, K. Blus, M. Gmurek, S. Ledakowicz, Coupling of electroco-agulation and ozone treatment for textile wastewater reuse, Chemical Engineering Journal 358 (2019) 992–1001.
[13] A.G. Khorram, N. Fallah, Treatment of textile dyeing factory wastewater by electrocoagulation with low sludge settling time : Optimization of operating parameters by RSM, Journal of Environmental Chemical Engineering 6 (2018) 635–642.
[14] L. Bilinska, K. Blus, M. Foszpanczyk, M. Gmurek, Catalytic ozonation of textile wastewater as a polishing step after industrial scale coagulation, Journal of Environmental Management 265 (2020) 110502.
[15] D. Donneys-Victoria, N. Marriaga-Cabrales, F. Machuca-Martínez, J. Benavides-Guerrero, S.G. Cloutier, Indigo carmine and chloride ions removal by electrocoagulation. Simultaneous production of brucite and layered double hydroxides, Journal of Water Process Engineering 33 (2020) 101106.
[16] A.L. Müller, E. Eyng, C. Lionço, S. de Oliveira, A.A. de Almeida, M.R. Fagundes-Klen, E. Sehn, Spectral deconvolution associated to the Gaussian fit as a tool for the optimization of photovoltaic electrocoagulation applied in the treatment of textile dyes, Science of the Total Environment 713 (2020) 136301.
[17] J. Núñez, M. Yeber, N. Cisternas, R. Thibaut, P. Medina, C. Carrasco, Application of electrocoagulation for the efficient pollutants removal to reuse the treated wastewater in the dyeing process of the textile industry, Journal of Hazardous Materials 371 (2019) 705–711.
[18] J.M. Aquino, G.F. Pereira, R.C. Rocha-Filho, N. Bocchi, S.R. Biaggio, Electrochemical degradation of a real textile effluent using boron-doped diamond or (-PbO_2 as anode, Journal of Hazardous Materials 192 (2011) 1275–1282.
[19] E. Yuksel, M. Eyvaz, E. Gurbulak, Electrochemical treatment of colour index reactive orange 84 and textile wastewater by using stainless steel and iron electrodes, Environmental Progress & Sustainable Energy 32 (2013) 60–68.
[20] M.M. Emamjomeh, M. Sivakumar, Review of pollutants removed by electrocoagulation and electrocoagulation/flotation processes, Journal of Environmental Management 90 (2009) 1663–1679.
[21] A. Aouni, C. Fersi, M. Ben Sik Ali, M. Dhahbi, Treatment of textile wastewater by a hybrid electrocoagulation/nanofiltration process, Journal of Hazardous Materials 168 (2009) 868–874.
[22] M. Bayramoglu, M. Kobya, O.T. Can, M. Sozbir, Operating cost analysis of electrocoagulation of textile dye wastewater, Separation and Purification Technology 37 (2004) 117–125.
[23] J. Nepo, B. Gourich, M. Cha, Y. Stiriba, C. Vial, P. Drogui, J. Naja, Electrocoagulation process in water treatment : A review of electroco-agulation modeling approaches, Desalination 404 (2017) 1–21.
[24] Y. Zhou, J. Lu, Y. Zhou, Y. Liu, Recent advances for dyes removal using novel adsorbents: A review, Environmental Pollution 252 (2019) 352–365.
[25] S.H. Chang, K.S. Wang, H.H. Liang, H.Y. Chen, H.C. Li, T.H. Peng, Y.C. Su, C.Y. Chang, Treatment of Reactive Black 5 by combined electrocoagulation granular activated carbon adsorption microwave regeneration process, Journal of Hazardous Materials 175 (2010) 850–857.
[26] O. Can, M. Kobya, E. Demirbas, M. Bayramoglu, Treatment of the textile wastewater by combined electrocoagulation, Chemosphere 62 (2006) 181–187.
[27] American Public Health Association (APHA), American Water Works Association (AWWA), Water Environmental Federation (WEF), 22nd edition, Standard methods for the examination of water and wastewater, American Public Health Association, Washington, D.C, 2012.
[28] L. Manfra, S. Canepa, V. Piazza, M. Faimali, Lethal and sublethal endpoints observed for Artemia exposed to two reference toxicants and an ecotoxicological concern organic compound, Ecotoxicology and Environmental Safety 123 (2016) 60–64.
[29] B.M. da Costa Filho, V.M. da Silva, J.d.O. Silva, A.E. da Hora Machado, A.G. Trovo, Coupling coagulation, flocculation and decantation with photo-Fenton process for treatment of industrial wastewater containing fipronil: Biodegradability and toxicity assessment, Journal of Environmental Management 174 (2016) 71–78.
[30] V. Sarria, S. Parra, N. Adler, P. Pringer, N. Bentez, C. Pulgarin, Recent developments in the coupling of photoassisted and aerobic biological processes for the treatment of biorecalcitrant compounds, Catalysis Today 76 (2002).
[31] E. GilPavas, S. Correa-Sainchez, Optimization of the heterogeneous electro-Fenton process assisted by scrap Zero-Valent iron for treating textile wastewater: Assessment of toxicity and biodegradability, Journal of Water Process Engineering 32 (2019) 100924.
[32] E. GilPavas, S. Correa-Sanchez, D.A. Acosta, Using scrap zero valent iron to replace dissolved iron in the fenton process for textile wastewater treatment: Optimization and assessment of toxicity and biodegradability, Environmental Pollution 252 (2019) 1709–1718.
[33] S. He, W. Sun, J. Wang, L. Chen, Y. Zhang, J. Yu, Enhancement of biodegradability of real textile and dyeing wastewater by electron beam irradiation, Radiation Physics and Chemistry 124 (2016) 203–207 13th Tihany Symposium on Radiation Chemistry.
[34] P. Lai, H.Z. Zhao, C. Wang, J.R. Ni, Advanced treatment of coking wastewater by coagulation and zero-valent iron processes, Journal of Hazardous Materials 147 (2007) 232–239.
[35] C. Wei, H. Wu, Q. Kong, J. Wei, C. Feng, G. Qiu, C.-H. Wei, F. Li, Residual chemical oxygen demand (cod) fractionation in bio-treated coking wastewater integrating solution property characterization, Journal of Environmental Management 246 (2019) 324–333.
[36] K. Ravndal, E. Opsahl, A. Bagi, R. Kommedal, Wastewater characterization by combining size fractionation, chemical composition and biodegradability, Water Research 131 (2018) 151–160.
[37] T. Tavangar, J. Kamran, M. Amin, A. Shahmirzadi, M. Karimi, Toward real textile wastewater treatment : Membrane fouling control and effective fractionation of dyes/inorganic salts using a hybrid electrocoagulation Nano filtration process, Separation and Purification Technology 216 (2019) 115–125.
[38] D.C. Montgomery, Design and analysis of experiments, John Wiley & sons, 2017.
[39] R.I. Kabacoff, R in action: Data analysis and graphics with R, (2011).
[40] N. Nippatla, L. Philip, Electrocoagulation-floatation assisted pulsed power plasma technology for the complete mineralization of potentially toxic dyes and real textile wastewater, Process Safety and Environmental Protection 125 (2019) 143–156.
[41] E. GilPavas, I. Dobrosz-Giomez, M.A. Giomez-Garcia, Optimization and toxicity assessment of a combined electrocoagulation, H_2O_2/ Fe^{2+}/UV and activated carbon

adsorption for textile wastewater treatment, Science of The Total Environment 651 (2019) 551–560.
[42] G. Varank, H. Sari, S. Yazc, A. Demir, G. Onkal Engin, Electrocoagulation of tannery wastewater using monopolar electrodes: Process optimization by response surface methodology, International Journal of Environmental Research 8 (2014) 165–180.
[43] M. Snipes, D. Taylor, Model selection and akaike information criteria: An example from wine ratings and prices, Wine Economics and Policy 3 (2014).
[44] A. Amani-Ghadim, A. Olad, S. Aber, H. Ashassi-Sorkhabi, Comparison of organic dyes removal mechanism in electrocoagulation process using iron and aluminum anodes, Environmental Progress Sustainable Energy 32 (2013).
[45] V. Khandegar, A. Saroha, Electrocoagulation for the treatment of textile industry effluent-a review, Journal of environmental management 128C (2013) 949–963.
[46] G. Mouedhen, M. Feki, M. Wery, H. Ayedi, Behaviour of aluminum electrodes in electrocoagulation, Journal of hazardous materials 150 (2008) 124–135.
[47] M. Kobya, O. Can, M. Bayramolu, Treatment of textile wastewaters by electrocoagulation using iron and aluminum electrodes, Journal of hazardous materials 100 (2003) 163–178.
[48] M.-C. Wei, K.-S. Wang, C.-L. Huang, C.-W. Chiang, T.-J. Chang, S.-S. Lee, S.-H. Chang, Improvement of textile dye removal by electrocoagulation with low-cost steel wool cathode reactor, Chemical Engineering Journal 192 (2012) 3744.
[49] A. Trubetskaya, J. Kling, O. Ershag, T. Attard, E. Schrder, Removal of phenol and chlorine from wastewater using steam activated biomass soot and tire carbon black, Journal of Hazardous Materials 365 (2019).
[50] T. Venkatesha, R. Viswanatha, Y.A. Nayaka, C. Bk, Kinetics and thermodynamics of reactive and vat dyes adsorption on mgo nanoparticles, Chemical Engineering Journals 198199 (2012) 110.
[51] Y. He, X. Wang, J. Xu, J. Yan, Q. Ge, X. Gu, L. Jian, Application of integrated ozone biological aerated filters and membrane filtration in water reuse of textile effluents, Bioresource Technology 133 (2013) 150–157.